


# Optimal Microneedle Design for Drug Delivery Based on Insertion Force Experiments with Variable Geometry

Bummo Ahn 

**Abstract:** Microneedles, which prick micro holes in the stratum corneum (SC), are promising minimally invasive drug delivery devices alternating pills, conventional needles, or transdermal patches. However, the microneedle fabrication based on the optimal design has been studied rarely. In this paper, the forces required to insert microneedles into a skin model were measured over the various geometries in order to optimize the microneedle design. To measure the insertion force, the microneedles were fabricated with inclined UV lithography and hot embossing processes. The insertion force was measured with a custom-made dynamic displacement device which can measure and record the force of mN range loads. The insertion force is strongly related with tip angle and radius of tip's curvature. The insertion forces increase with increasing width of shaft, but the relation is very weak and the radius of fillet in the experimental range has no influence on the insertion force. This result can be used as an optimal design guide on the geometries of microneedle.

**Keywords:** Drug delivery, insertion force optimal microneedle design, variable geometry.

## 1. INTRODUCTION

The delivery of drugs into the human body orally is problematic mainly due to the degradation of drugs in the gastrointestinal tract and their elimination through the liver. Further, the delivery of drugs using conventional hypodermic needles is painful for patients and is not appropriate for long term, continuous deliveries [1–3]. An alternative delivery technique employs a transdermal patch. However, transdermal delivery is severely limited by the inability of a large majority of drugs to enter the body through the skin at therapeutic rates because the skin's outer layer (the stratum corneum) is approximately 10–20  $\mu\text{m}$  thick and is composed of keratinized dead cells and scales [4].

The skin permeability is increased enormously if the stratum corneum layer is disrupted. To disrupt the layer, a number of different approaches have been studied; they range from chemical/lipid enhancers [5,6] to electric fields employing iontophoresis and electroporation [7,8] to pressure waves generated by ultrasound or photoacoustic effects [9,10]. These enhancement methods have made only a limited impact on medical practices to date because chemical methods can affect the skin and the drug, and physical methods require complex systems. Microneedles, which are effective in forming micro perforations in the stratum corneum, do not cause chemical effects on

the skin or the drug and do not require an energy source or other complex systems [11–14]. Therefore, they are promising minimally invasive drug delivery devices alternating pills, conventional needles, or transdermal patches.

The microneedles are classified to solid or hollow ones. Although hollow microneedles can be applied to active drug deliveries or blood extractions, it is difficult to mass-produce them with biocompatible materials [15–17]. While solid microneedles can be only applied to passive drug deliveries, the solid microneedles have been recently made of cheap and biocompatible polymers [18–27]. Therefore, solid microneedles hold priority to hollow ones for reasonable passive drug delivery systems.

To apply for clinical application, the research on the optimal geometry design based on the insertion force and fracture force is very important. However, the mechanics of microneedle insertion force has been investigated by several groups [28–32]. Davis *et al.* performed insertion experiments using metal hollow microneedles whose full cross-sectional area, tip radius and wall thickness were inappropriate for drug delivery [28]. Zahn *et al.* were used the poly-silicone hollow microneedles and measured the fracture force against the applied side forces [29]. Stupar *et al.* measured the insertion forces of silicone hollow microneedles against a 400  $\mu\text{m}$  thick gelatin membrane [30]. They suggests the insertion force as 0.45 N on 4.5 mm length and 200  $\mu\text{m}$  width. Chandrasekaran *et*

Manuscript received March 28, 2019; revised July 24, 2019; accepted July 31, 2019. Recommended by Guest Editors Doo Yong Lee (KAIST) and Jaesoon Choi (Asan Medical Center). This journal was supported by the Bio & Medical Technology Development Program of the National Research Foundation (NRF) funded by the Korean Government (MSIP) (No. NRF-2017M3A9E2063101).

Bummo Ahn is with the Robotics R&BD Group, Korea Institute of Industrial Technology, Ansan si, Gyeonggi-do, 15588, Korea and with the Robotics & Virtual Engineering, KITECH Campus, Ansan si, Gyeonggi-do, 15588, Korea (e-mail: bmahn@kitech.re.kr).

*al.* used the metal hollow microneedles [31]. They performed the insertion experiments and measured the insertion force on the skin-like polymer (PS-4B, M-line Accessories Inc.). They suggested the insertion force as 80-90 mN on the microneedle (tip angle and thickness are  $30^\circ$  and  $10\ \mu\text{m}$ ). Park *et al.* measured the fracture forces against normal forces and side forces [32]. They show the shorter length and bigger diameter microneedles have bigger fracture force.

In this paper, experiments of polymer microneedle insertion into human skin model (injection trainer and high-density polyethylene film) are performed in order to optimize the microneedle geometries. The microneedles for the experiments are fabricated with inclined UV lithography and hot embossing processes. Furthermore, I designed and fabricated microneedles having different size of the front tip angle, the radius of tip's curvature, the width of shaft, and the radius of fillet. The insertion forces are measured with a custom-made dynamic displacement device which can measure and record the force of mN range loads.

## 2. MATERIALS AND METHODS

### 2.1. Microneedle fabrication processes and geometry

Fig. 1 illustrates the fabrication process of in-plane microneedles using SU-8 in inclined UV lithography and nickel-electroforming. First, a 150-nm-thick chromium (Cr) layer is deposited onto a Pyrex glass wafer (Corning). After the Cr layer is patterned to define the microneedle's shape, an SU-8 structure is formed on the Cr-patterned glass wafer by inclined UV lithography [19, 33–35]. After a titanium (Ti) layer is deposited as a seedlayer for electroplating, a Ni layer is formed on the entire upper surface of the wafer by electroplating. Then the Ni layer is stripped from the wafer. To obtain the final in-plane microneedles, the Ni sheet is polished to the desired thickness of the microneedles.

The fabrication process of polymer out-of-plane microneedles is shown in Fig. 2. First the in-plane microneedles are converted to an out-of-plane microneedle array using rectangular spacers which not only create spaces between the neighboring in-plane microneedles but also maintain these in-plane microneedles are tightly fixed to each other with screws. A negative mold is fabricated by replicating the out-of-plane microneedle array with polydimethylsiloxane (PDMS). Finally, out-of-plane microneedle sheets of biocompatible polymer are fabricated by using the negative mold in a hot embossing machine using polycarbonate (PC). The mold and PC grains are loaded the hot embossing machine, heated for 8 min at  $240^\circ\text{C}$ , pressed for 2 min with a load of  $10\ \text{kg}/\text{cm}^2$ . They are then unloaded from the machine in order to cool the mold and the polymer rapidly and pressed with a 5-kg metal block to prevent deformation. After the stack is

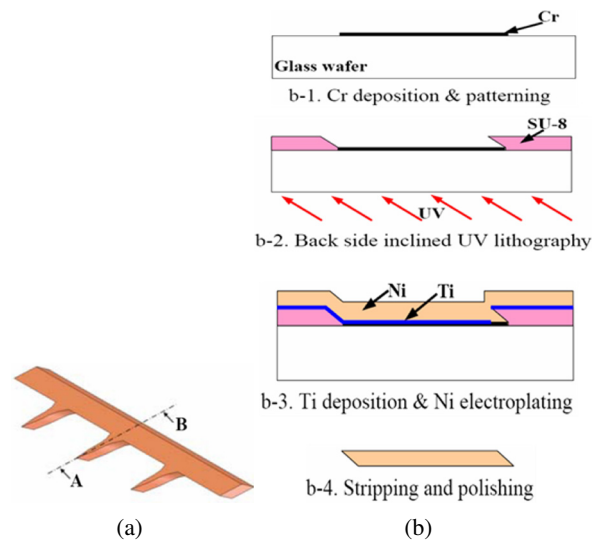


Fig. 1. Process for fabricating in-plane microneedles: (a) schematic view of single row microneedle array, (b) fabrication process along the cross-section along line A-B shown in (a).

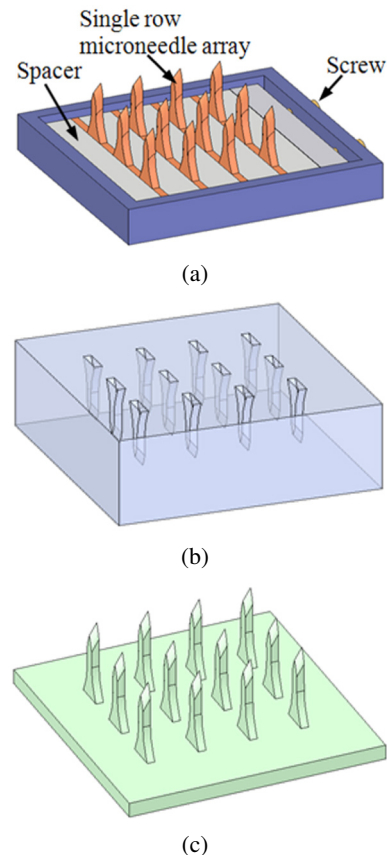


Fig. 2. Steps to fabricate polymer out-of-plane microneedles: (a) master mold for a punched on substrated solid microneedle sheet, (b) negative PDMS mold, (c) polymer microneedles.

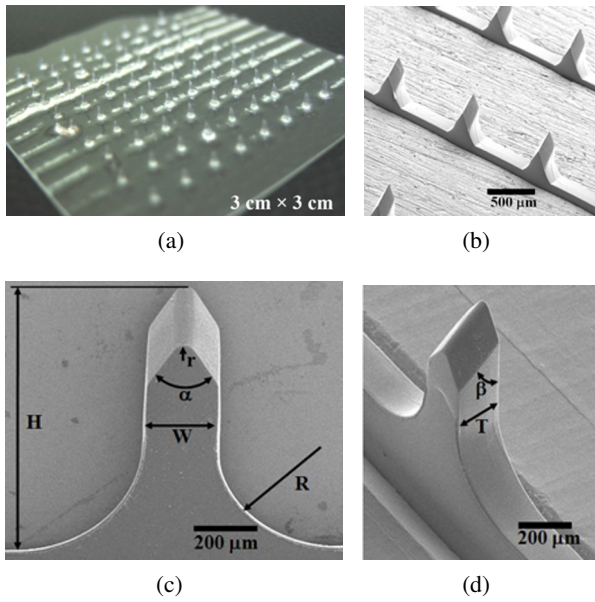


Fig. 3. Images of the PC out-of-plane microneedle: (a) photograph, (b) SEM image of array (isometric view), (c) Front view, (d) perspective view.

cooled for 5 min at room temperature, the PC microneedle sheet is demolded and the excess PC that has overflowed is cut off.

Fig. 3 shows the images of the PC out-of-plane microneedle; (a) shows the microneedle array sheet and (b)-(d) show the SEM images of the microneedles. The heights of the microneedles range from 0.8 mm to 1.5 mm. The  $w$  is the width and  $t$  is the thickness, respectively. The  $\alpha$  is the front angle and side angle is  $\beta$ . The fabricated in-plane microneedles have a sharp tip and are long; thus a low insertion force is required and sufficient penetration depth is achieved. The needle density can be increased by converting the in-plane microneedles to an out-of-plane microneedle array; this results in sufficient drug delivery rates. The microneedle sheet fabricated by the process is mass-producible and biocompatible. In addition, it has three-dimensional sharp tips, dense needle density and sufficient shaft length. Thus, the punched-on-substrate solid microneedle sheet which will be fabricated by modifying the process will be mass-producible and biocompatible and have three-dimensional sharp tips, dense needle density and sufficient shaft length, so the microneedle sheet will be cheap and safe and have a low insertion force, a sufficient delivery rate and a sufficient penetration depth.

The microneedles were prepared in order to perform the experiments on the microneedle insertion force [10]. The standard microneedle geometries are followed; the height ( $H$ ) is  $790 \pm 20 \mu\text{m}$ , the thickness ( $T$ ) is  $160 \pm 5 \mu\text{m}$ , the side tip angle ( $\beta$ ) is 40 degree, the  $\alpha$  is 60 degree, the

Table 1. Geometry information of the microneedle.

Dimensions (units)	Standard geometry	Variable geometry
$H (\mu\text{m})$	$790 \pm 20$	
$W (\mu\text{m})$	220	110, 160, 220, 280, 330
$T (\mu\text{m})$	$160 \pm 5$	
$R (\mu\text{m})$	350	75, 150, 350, 450, 550
$r (\mu\text{m})$	35	10, 15, 35, 70, 110
$\alpha (^\circ)$	60	40, 60, 70, 130
$\beta (^\circ)$	40	

$r$  is  $35 \mu\text{m}$ , the  $W$  is  $220 \mu\text{m}$ , and the  $R$  is  $350 \mu\text{m}$ . The variable microneedle geometries are as followed; the front tip angles ( $\alpha$ ) of 40, 60, 70, 130, and 180 degrees, the radius of tip's curvature ( $r$ ) of 10, 15, 35, 70, and  $110 \mu\text{m}$ , the width of shaft ( $W$ ) of 110, 160, 220, 280, and  $330 \mu\text{m}$ , and the radius of fillet ( $R$ ) at base of 75, 150, 350, 450, and  $550 \mu\text{m}$ . Table 1 shows the geometry information of the fabricated microneedles.

## 2.2. Experimental setup and procedure

To study the insertion force of microneedles, I built an experimental setup composed of a dynamic displacement device, a control board and a PC [36, 37]. The displacement device is consists of a motor (Maxon Precision motors, Fall River, USA), a force transducer (Senstech co., LTD. Korea), and a probe attached a microneedle. It can apply dynamic displacement of the microneedle, which attaches the probe to the tissue model as shown in Fig. 4. The resolution of the force sensor is 0.7 mN and its measurement range is from 0 mN to 9.8 kN. The maximum errors of the probe's positions compared to input values are less than  $5 \mu\text{m}$  by calibrating the dynamic motion of the DC motor. The probe's displacement range is up to 41.5 mm, and the maximum speed is 8 mm/s. The device can induce unit step, sine, rectangular and saw tooth wave inputs of about  $10 \mu\text{m}$  - 41.5 mm displacements.

To validate the biocompatibility of our microneedle, it is desirable that the experiments were carried out using the human skin. However, there are several limitations for the experiments on human skin. First, it is possible to infect the human subject through the microneedle that is contaminated by the virus and other materials. Second, it is difficult to measure the precise insertion forces from the human subject even if there is a tiny movement of the subject it can make a serious error of results. Finally, it is hard to perform the experiments repetitively. Therefore, I choose a human skin phantom that consisted of a 30 mm-thick high-density polyethylene film as the stratum corneum and an injection trainer (Limbs & Things, Ltd. UK) as the epidermis and dermis.

Microneedle insertion experiments were performed on the human skin model. The microneedle is attached to

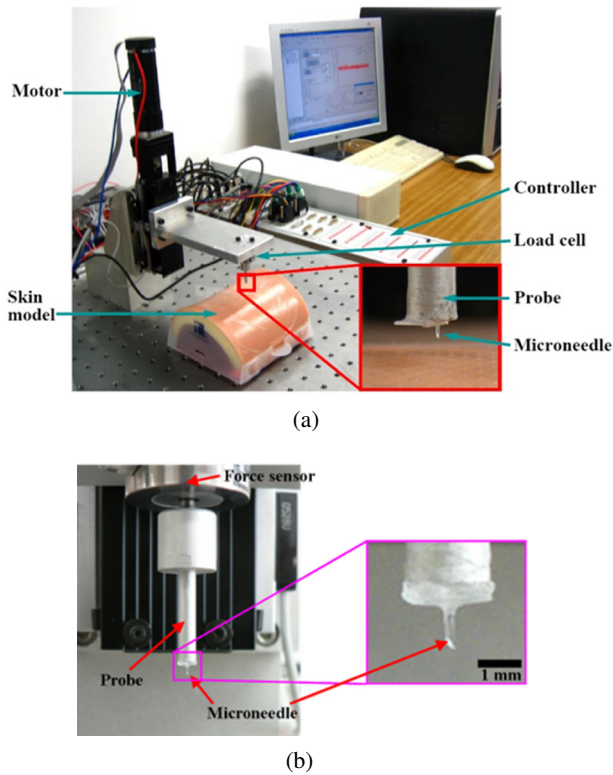
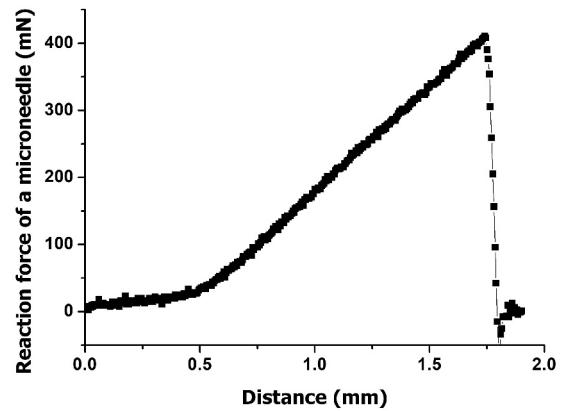


**Fig. 4.** (a) Experimental setup for measuring microneedle insertion force during insertion against human skin phantom (Injection Trainer + polyethylene film), (b) probe attached microneedle for microneedle insertion experiments.

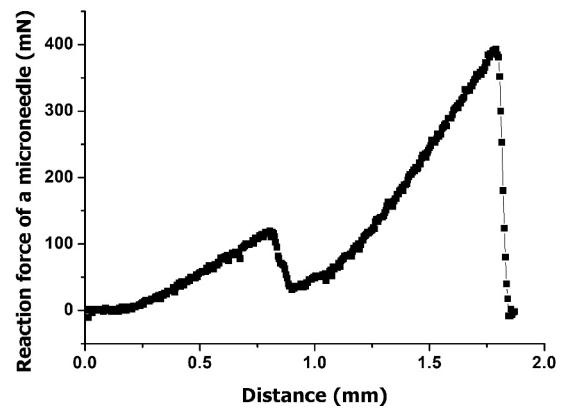
the probe that is connected to the force sensor as shown in Fig. 4(b). The experimental procedures are as follow. First, the probe was moved close to the surface of the tissue model and the microneedle tip was contacted to the surface through the reaction force profile change. Second, the insertion profile of sawtooth waves (amplitude: 1 mm, velocity: 100  $\mu\text{m}/\text{sec}$ ) was applied to the model and the insertion force was measured by the force sensor. Third, the data of the insertion force and displacement were acquired with the data acquisition board (D-space) and stored in the PC. Finally, the experimental sites of human skin model were changed after puncturing by the microneedle.

### 3. RESULTS

The reaction force profiles of the experiments were measured using the experimental setup. The reaction force of the injection trainer alone is shown in Fig. 5(a). The reaction force obtained from the human skin model was increased along with the range of the needle insertion. When the needle penetrated the polyethylene film, the force was dropped suddenly and increased again (Fig. 5(b)). The in-



(a)



(b)

**Fig. 5.** Reaction force profiles of a microneedle for penetrating the human skin model: (a) Injection trainer alone and (b) Plastic film on injection trainer.

sertion force of the microneedle is the point just before sudden drop of the reaction force that can be used to compare the insertion forces obtained by the other microneedles with different geometries. The measured profile is similar to that of reaction force during microneedle insertion into the stratum corneum of a human subject in the previous experiment [11]. Therefore, the used human skin model is appropriate to measure the similar insertion forces of the human skin.

Fig. 6 shows the insertion forces as functions of microneedle's geometries. The insertion forces increase strongly with increasing tip angle up to 130 degree and decrease slightly at 180 degree at which the tip acts as the edge of a knife. Large radius of tip's curvature induces large insertion force, but if the radius is smaller than 35  $\mu\text{m}$ , the effect is not dominant. The insertion forces increase with increasing width of shaft. The radius of fillet in the experimental range has no influence on the insertion force.



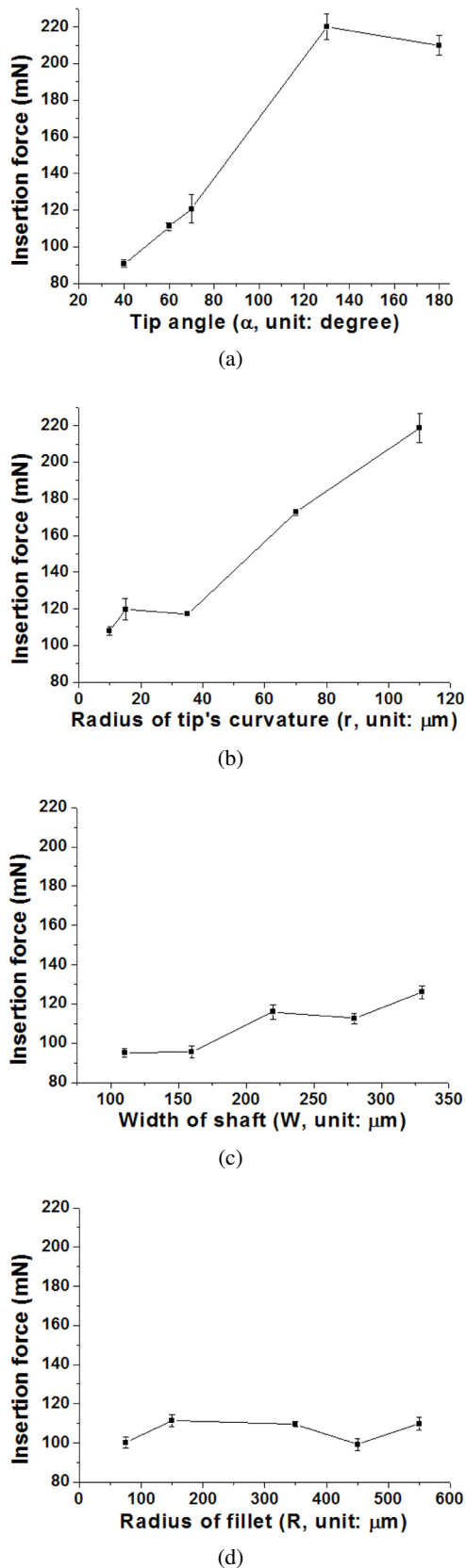


Fig. 6. Insertion forces as functions of microneedle's geometries.

#### 4. DISCUSSION AND CONCLUSION

Microneedles, which are effective to form micro perforations in the stratum corneum (the outer skin layer), are one of the promising minimally invasive drug delivery devices alternating pills, conventional needles, or transdermal patches. However, microneedles are not commercialized by this time because of weak needle structure, low mass-productivity or bio-incompatibility. To overcome the limitations of the previous microneedles, I fabricated microneedles using novel fabrication process that consists of inclined UV lithography and polymer molding process. The biocompatible polymer with a hot embossing process can be used to fabricate the microneedle. In addition, I fabricated microneedles with the various front tip angles, radius of tip's curvature, width of shaft, and radius of fillet. The single row microneedles are fabricated with a sharp tip for low insertion forces and are made long to ensure sufficient penetration depth. The single row microneedles are converted into an out-of-plane type multi row microneedle array to increase the needle density. The negative mold is fabricated for mass- production using a polymer molding technique. The final out-of-plane microneedle sheets are produced using polycarbonate for biocompatibility by employing the hot embossing process.

To design the optimal geometries of the microneedles, I studied the insertion forces of the microneedles with variable geometry. Therefore, the force required to insert the microneedles into a skin model, Injection Trainer covered with a thin plastic film, was measured.

The reaction force profile piercing the skin model through the fabricated microneedle is similar to that piercing the living skin. Over the range of microneedle geometries investigated, insertion forces obtained from the experiments ranged from about 100 to 200 mN. The insertion forces are strongly related with tip angle and radius of tip's curvature. In addition, the width of shaft is slightly affected to the insertion forces and has a linear relationship with the insertion force. Therefore, these results can be used to decide the optimal microneedle geometry in order to puncture the human outer skin layer (stratum corneum) without any fracture of microneedle.

#### REFERENCES

- [1] R. Langer, "Drug delivery and targeting," *Nature*, vol. 392, pp. 5-10, 1998.
- [2] K. Park, "Controlled drug delivery: challenges and strategies," *American Chemical Society*, Washington, DC, 1997.
- [3] A. L. Teo, C. Shearwood, K. C. Ng, J. Lu, and S. Moochhala, "Transdermal microneedles for drug delivery applications," *Materials Science and Engineering: B*, vol. 132, pp. 151-154, 2006.
- [4] K. A. Holbrook and G. F. Odland, "Regional differences in the thickness (cell layers) of the human stratum corneum:

- an ultrastructural analysis," *Journal of Investigative Dermatology*, vol. 62, pp. 415-422, 1974.
- [5] A. C. Williams and B. W. Barry, "Penetration enhancers," *Advanced Drug Delivery Reviews*, vol. 56, pp. 603-618, 2004.
- [6] G. Cevc, "Lipid vesicles and other colloids as drug carriers on the skin," *Advanced Drug Delivery Reviews*, vol. 56, pp. 675-711, 2004.
- [7] Y. N. Kalia, A. Naik, J. Garrison, and R. H. Guy, "Iontophoretic drug delivery," *Advanced Drug Delivery Reviews*, vol. 56, pp. 619-658, 2004.
- [8] A. R. Denet, R. Vanbever, and V. Preat, "Skin electroporation for transdermal and topical delivery," *Advanced Drug Delivery Reviews*, vol. 56, pp. 659-674, 2004.
- [9] A. G. Doukas and N. Kolloas, "Transdermal delivery with a pressure wave," *Advanced Drug Delivery Reviews*, vol. 56, pp. 559-579, 2004.
- [10] S. Mitragotri and J. Kost, "Low-frequency sonophoresis: a review," *Advanced Drug Delivery Reviews*, vol. 56, pp. 589-601, 2004.
- [11] S. Henry, D. McAllister, M. G. Allen, and M. R. Prausnitz, "Microfabricated microneedles: a novel method to increase transdermal drug delivery," *Journal of Pharmaceutical Sciences*, vol. 87, pp. 922-925, 1998.
- [12] H. Lee, C. Song, Y. S. Hong, M. S. Kim, H. R. Cho, T. Kang, K. Shin, S. H. Choi, T. Hyeon, and D. H. Kim, "Wearable/disposable sweat-based glucose monitoring device with multistage transdermal drug delivery module," *Science Advances*, vol. 3, e1601314, 2017.
- [13] Y. Chen, B. Z. Chen, Q. L. Wang, X. Jin, and X. D. Guo, "Fabrication of coated polymer microneedles for transdermal drug delivery," *Journal of Controlled Release*, vol. 265, pp. 14-21, 2017.
- [14] K. Cheung and D. B. Das, "Microneedles for drug delivery: trends and progress," *Drug Delivery*, vol. 23, no. 7, pp. 2338-2354, 2016.
- [15] S. J. Moon and S. S. Lee, "A novel fabrication method of a microneedle array using inclined deep X-ray exposure," *Journal of Micromechanics and Microengineering*, vol. 15, pp. 903-911, 2005.
- [16] S. J. Moon, S. S. Lee, H. S. Lee, and T. H. Kwon, "Fabrication of microneedle array using LIGA and hot embossing process," *Microsystem Technology*, vol. 11, pp. 311-318, 2005.
- [17] J. M. Lippmann, E. J. Geiger, and A. P. Pisano, "Polymer investment molding: method for fabricating hollow, microscale parts," *Sensors and Actuators A-Physics*, vol. 134, pp. 2-10, 2007.
- [18] J. H. Park, M. G. Allen, and M. R. Prausnitz, "Biodegradable polymer microneedles: fabrication, mechanics and transdermal drug delivery," *Journal of Controlled Release*, vol. 104, pp. 51-66, 2005.
- [19] M. Han, D. H. Hyun, H. H. Park, S. S. Lee, C. H. Kim, and C. G. Kim, "A novel fabrication process for out-of-plane microneedle sheets of biocompatible polymer," *Journal of Micromechanics and Microengineering*, vol. 17, pp. 1184-1191, 2007.
- [20] S. M. Bal, A. C. Kruithof, R. Zwier, E. Dietz, J. A. Bouwstra, J. Lademann, and M. C. Meinke, "Influence of microneedle shape on the transport of a fluorescent dye into human skin in vivo," *Journal of Controlled Release*, vol. 147, pp. 218-224, 2010.
- [21] S. M. Bal, B. Slütter, W. Jiskoot, and J. A. Bouwstra, "Small is beautiful: N-trimethyl chitosan-ovalbumin conjugates for microneedle-based transcutaneous immunization," *Vaccine*, vol. 29, pp. 4025-4032, 2011.
- [22] S. M. Bal, B. Slütter, E. Riet, A. C. Kruithof, Z. Ding, G. F. A. Kersten, W. Jiskoot, and J. A. Bouwstra, "Efficient induction of immune responses through intradermal vaccination with N-trimethyl chitosan containing antigen formulations," *Journal of Controlled Release*, vol. 142, pp. 374-383, 2010.
- [23] F. Chabri, K. Bouris, T. Jones, D. Barrow, A. Hann, C. Allender, K. Brain, and J. Birchall, "Microfabricated silicon microneedles for nonviral cutaneous gene delivery," *British Journal of Dermatology*, vol. 150, pp. 869-877, 2004.
- [24] H. Kalluri, C. S. Kolli, and A. K. Banga, "Characterization of microchannels created by metal microneedles: formation and closure," *The AAPS Journal*, vol. 13, pp. 473-481, 2011.
- [25] B. Slütter, S. M. Bal, D. Zhi, W. Jiskoot, and J. A. Bouwstra, "Adjuvant effect of cationic liposomes and CpG depends on administration route," *Journal of Controlled Release*, vol. 154, pp. 123-130, 2011.
- [26] S. L. Banks, K. S. Paudel, N. K. Brogden, C. D. Loftin, and A. L. Stinchcomb, "Diclofenac enables prolonged delivery of naltrexone through microneedle-treated skin," *Pharmaceutical Research*, vol. 28, pp. 1211-1219, 2011.
- [27] K. Van der Maaden, E. Sekerdag, W. Jiskoot, and J. Bouwstra, "Impact-insertion applicator improves reliability of skin penetration by solid microneedle arrays," *The AAPS Journal*, vol. 16, pp. 681-685, 2014.
- [28] S. P. Davis, B. J. Landis, Z. H. Adams, M. G. Allen, and M. R. Prausnitz, "Insertion of microneedles into skin: measurement and prediction of insertion force and needle fracture force," *Journal of Biomechanics*, vol. 37, pp. 1155-1163, 2004.
- [29] J. D. Zahn, N. H. Talbot, D. Liepmann, and A. P. Pisano, "Microfabricated polysilicon microneedles for minimally invasive biomedical devices," *Biomedical Microdevices*, vol. 2, pp. 295-303, 2000.
- [30] P. A. Stupar and A. P. Pisano, "Silicon, parylene, and silicon/parylene micro-needles for strength and toughness," *Transducers'01*, Munich, Germany, pp. 1358-1361, 2001.
- [31] S. Chandrasekaran and A. B. Frazier, "Characterization of surface micromachined metallic microneedles," *Journal of Microelectromechanical Systems*, vol. 12, pp. 289-295, 2003.
- [32] J.H. Park, M.G. Allen, and M.R. Prausnitz, "Biodegradable polymer microneedles: fabrication, mechanics and transdermal drug delivery," *Journal of Controlled Release*, vol. 104, pp. 51-66, 2005.

- [33] M. Han, W. Lee, S. K. Lee, and S. S. Lee, "Microfabrication of 3D oblique structures by inclined UV lithography," *Proc. of microTAS 2002*, vol. 1, pp. 106-108, 2002.
- [34] Y. K. Yoon, J. H. Park, F. Cros, and M. G. Allen, "Integrated vertical screen microfilter system using inclined SU-8 Structures," *Proc. of IEEE Conf. MEMS*, Kyoto, Japan, pp. 227-230, 2003.
- [35] H. Sato, T. Kakinuma, J. S. Go, and S. Shoji, "A novel fabrication of in-channel 3-D micromesh structure using maskless multi-angle exposure and its microfilter application," *Proc. of IEEE Conf. MEMS*, Kyoto, Japan, pp. 223-226, 2003.
- [36] B. Ahn and J. Kim, "Measurement and characterization of soft tissue behavior with surface deformation and force response under large deformations," *Medical Image Analysis*, vol. 14, pp. 138-148, 2010.
- [37] B. Ahn and J. Kim, "Efficient soft tissue characterization under large deformations in medical simulations," *International Journal of Precision Engineering and Manufacturing*, vol. 10, pp. 115-121, 2009.



**Bummo Ahn** received his masters and Ph.D. degrees from the Department of Mechanical Engineering, Korea Advanced Institute of Science and Technology, Daejeon, Korea, in 2007 and 2011, respectively. He is currently a Principal Researcher of the Robotics Research and Development Group, Korea Institute of Industrial Technology, Ansan, Korea. He is also appointed as an Associate Professor with the Robotics and Virtual Engineering, University of Science and Technology, Daejeon, Korea. His current research interests include medical robotics, biomechanics, and rehabilitation.

**Publisher's Note** Springer Nature remains neutral with regard to jurisdictional claims in published maps and institutional affiliations.